

Effect of rolling speed on the occurrence of strain aging during and after warm rolling of a low-carbon steel

B. Koohbor · D. Ohadi · S. Serajzadeh ·

J. M. Akhgar

Received: 15 August 2009 / Accepted: 1 March 2010 / Published online: 18 March 2010
© Springer Science+Business Media, LLC 2010

Abstract In this study, effect of rolling speed on strain aging phenomena in warm rolling of a carbon steel has been investigated. For this purpose, by using a mathematical model and predicting temperature and strain rate fields, the possibility of occurrence of dynamic strain aging during the warm rolling was first evaluated. In the next stage, warm-rolled samples were aged up to 11 months at room temperature for studying the kinetics of static strain aging, while mechanical tests as well as microstructural evolutions have been performed to determine the effect of strain aging on material behavior. The results indicate that dynamic strain aging may not occur for the employed rolling program; however, static strain aging takes place after warm rolling leading to changes in the mechanical behavior of the warm-deformed samples. In addition, by increasing rolling speed, the aging time required to achieve the maximum hardness increases.

Introduction

Warm rolling process has recently been considered in steel shaping industries because of its production advantages and lower production costs [1]. However, the phenomenon of strain aging may occur during and after warm rolling process and significantly affect the mechanical properties of the steel products. Static strain aging (SSA) in low-carbon steels is the result of an interaction between the dislocations and interstitial atoms [2, 3]. When pre-strained specimens of low-carbon steel are aged at low

temperatures, the kinetic energy gained by the solute carbon atoms cause them to diffuse to the dislocations and immobilize them. Therefore, strain aging leads to an increase in flow stress of the aged metal as well as to the appearance of yield point phenomenon recognized as Luders bands [3, 4]. Another metallurgical phenomenon that shows itself as a serrated stress–strain curve is known as dynamic strain aging (DSA) [4]. The occurrence of DSA is mainly observed due to the periodic locking and unlocking of dislocations by interstitial or substitutional atoms [4].

Static strain aging and its effect on the mechanical behavior of steels has been studied in several works [5–8]. Multistage strain aging and its effect on the flow behavior and mechanical properties of a low-carbon steel is studied by Staiger et al. [5]. In this work, it is concluded that the strain aging history of the aged samples may have significant effects on the aging behavior of the samples. Pan et al. [6] have studied the strain rate and aging effect on the mechanical properties of steel sheets. Effects of strain aging on the mechanical behavior and workability of low-carbon steels have been studied by Taheri et al. [7, 8]. Other works have also been carried out on the effect of aging on different grades of steels, i.e., dual phase steels and low-alloy steels [9, 10]. Dynamic strain aging and its effect on mechanical behavior of carbon steels have also been investigated in several researches [11–13]. Accordingly, it is shown that DSA may occur during the warm deformation operations depending on the employed working conditions.

In this study, effect of rolling speed on the occurrence of strain aging in a low-carbon steel is investigated. First, the possibility of occurrence of DSA during the warm rolling process is determined by means of a mathematical model for prediction of temperature and strain rate fields together

B. Koohbor · D. Ohadi · S. Serajzadeh (✉) · J. M. Akhgar
Department of Materials Science and Engineering, Sharif University of Technology, Azadi Ave, Tehran, Iran
e-mail: serajzadeh@sharif.edu

with the experimental $\ln(\dot{\varepsilon})$ vs. T^{-1} plot. Then, the kinetics of SSA and the effect of rolling speeds are studied. For this purpose, warm rolling experiments with various rolling speeds are performed on steel samples. The rolled samples are then aged naturally for periods of 17 days to 11 months. After that, tensile and hardness tests are carried out in order to evaluate the mechanical properties of the aged samples. In this way, the occurrence of SSA and the effect of rolling speed on this phenomenon are studied.

Mathematical model

During warm rolling of low-carbon steels, DSA may take place and affect the flow behavior of the rolled products [14]. In order to determine the occurrence of DSA, a two-dimensional mathematical model has been utilized to predict the temperature, strain rate fields within the metal being rolled. To do so, the heat conduction equation has been solved within the rolled metal. The governing heat transfer equation used in this analysis has been expressed as Eq. 1,

$$\nabla(k\nabla T) + \dot{Q} = \rho c \frac{\partial T}{\partial t}, \quad (1)$$

where in this equation ρ , c , and k are density, specific heat, and thermal conductivity of the rolling strip, respectively, and \dot{Q} represents the rate of heat of deformation. In the deformation zone, two distinct boundary conditions can be recognized, the contact area of strip and work-roll and the area at which the strip has no contact to work-roll and heat transfers to atmosphere mainly by convection through the strip surface as schematically displayed in Fig. 1. In addition, at the contact area, a distributed surface flux, q_{fric} , is generated from frictional sliding which is determined as [14]:

$$q_{\text{fric}} = \tau A_c |v| \delta t, \quad (2)$$

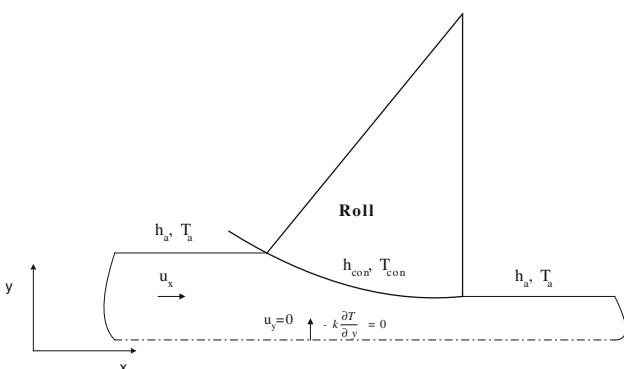


Fig. 1 Illustration of roll gap geometry and the governing boundary conditions

where $|v|$ is the relative velocity between the metal and the work-roll, δt the applied time-step, A_c the contact area, and τ the frictional stress. The boundary condition in deformation zone can be expressed as

$$-k \frac{\partial T}{\partial n} = h_{\text{con}}(T - T_r) - q_{\text{fric}}, \quad (3)$$

where “n” denotes normal direction to the surface boundary, T_r is the work-roll surface temperature that can be calculated simultaneously by solving the governing heat conduction equation of the work-roll, and h_{con} the interface heat transfer coefficient, which has been calculated as a function of rolling pressure by Eq. 4 [15]:

$$h_{\text{con}} = 0.695P - 34.4, \quad (4)$$

where P is the pressure in MPa and h_{con} the coefficient of heat transfer in $\text{kW/m}^2 \text{C}$. The other boundary condition used to express the heat transfer by convection, outside the deformation zone is

$$-k \frac{\partial T}{\partial n} = h_a(T - T_a). \quad (5)$$

In Eq. 5, T_a represents surrounding temperature, and h_a is the convection heat transfer coefficient to surrounding. To evaluate the rate of heat of deformation in the heat conduction equation, strain rate field as well as the roll pressure, it is required to determine the velocity field in the metal during rolling experiments. A two-dimensional dynamic coupled temperature–displacement analysis based on updated Lagrangian formulation has been employed to simulate strip rolling process. In the present work, viscoplastic material laws have been taken into account and because of the symmetric characteristics of the process only the upper half of the setup has been included. From Hamilton’s principle for a volume V with surface S , the increment in virtual work per unit volume and per unit time can be written as follow [16]:

$$\delta W = \int_V \rho \ddot{\mathbf{u}} \cdot \delta \mathbf{v} \, dV + \int_V \boldsymbol{\sigma} : \delta \mathbf{D} \, dV - \int_S \mathbf{t} \cdot \delta \mathbf{v} \, dS = 0 \quad (6)$$

Here $\ddot{\mathbf{u}}$, $\delta \mathbf{v}$, and \mathbf{t} are the acceleration, virtual velocity, and traction vectors, respectively, $\boldsymbol{\sigma}$ the stress tensor, and $\delta \mathbf{D}$ is the virtual deformation rate tensor. The frictional coefficient is assumed to be constant during deformation and its direction is opposite to the direction of the relative velocity at the contact surface. Also it should be noted that in order to evaluate the flow stress behavior of rolled strips, the “power-law” equation has been considered as:

$$\sigma = B \dot{\varepsilon}^m \varepsilon^n, \quad (7)$$

where σ is the instantaneous flow stress of the rolled metal, B the strength coefficient, $\dot{\varepsilon}$ and ε the true strain and true

strain rate, respectively, while n and m are work hardening and strain rate sensitivity factors, respectively. Note that the flow stress data in ref. [14] have been employed to assess the above-mentioned coefficients.

The above integrated thermo-mechanical model is performed using ABAQUS [17]. It is worth noting that four-node iso-parametric elements are employed in the finite-element analysis assuming plane strain conditions, while the total number of elements used in the model are chosen to be 1190 of type CPE4RT including 7 elements in the thickness direction and 170 in the length of the rolled strip.

Also, in order to examine the possibility of the occurrence of DSA, the Arrhenius-type equation has been used as follows [2]:

$$\dot{\varepsilon} = A \exp(-Q/RT), \quad (8)$$

where A is the frequency factor, R the gas constant, and Q the activation energy required for serrated flow (DSA).

Table 1 Chemical composition of the steel employed in this study

C (wt%)	Mn (wt%)	S (wt%)	P (wt%)	N (ppm)
0.08	0.85	0.003	0.003	120

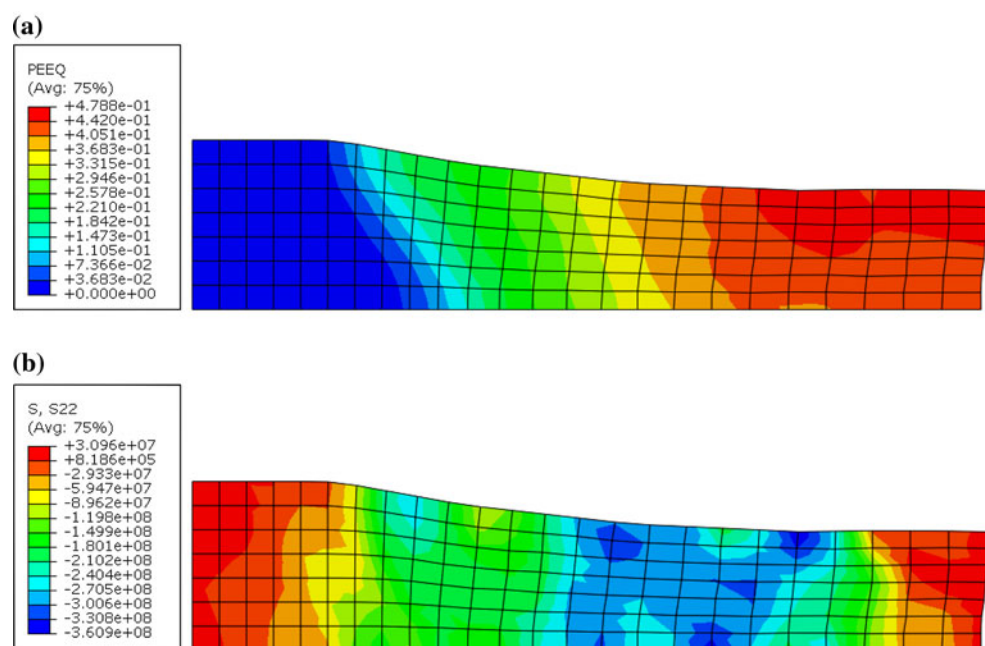
Table 2 Strip thicknesses in different stages of warm rolling experiments

Thickness of the initial strip (mm)	10
Thickness of the strip, after the first pass (mm)	7.8
Thickness of the strip, after the second pass (mm)	6.3
Thickness of the strip, after the third pass (mm)	5

Experimental procedure

In this work, warm strip rolling of a low-carbon steel with the chemical composition listed in Table 1 was examined. The rolling samples were machined out of the as-received hot-rolled bars. The dimensions of the samples used for the warm rolling experiments were chosen to be $10 \times 50 \times 100$ mm³, and the work-roll diameter was 150 mm. All samples were first heated up to 870 °C, held for 10 min at this temperature, and then the warm rolling experiments were performed. Reduction of 50% and rolling speeds of 43, 50, 64, and 71 rpm were employed in the warm rolling experiments. The total reduction of 50% was achieved in three successive passes with inter-pass time of 2 s, and after warm rolling, the samples were cooled down to ambient temperature in still air. Table 2 shows the strip thickness in different stages of warm rolling experiments. After the warm rolling experiments, the tensile samples were prepared according to ASTM-E8M. The tensile tests were carried out at the room temperature and the constant cross-head speed of 2 mm min⁻¹, equivalent to nominal strain rate of 10^{-3} s⁻¹. The hardness tests were performed utilizing the Vickers hardness testing on the surface of samples. The first series of mechanical tests were performed after 17 days. Three other samples were aged for the periods of 4–11 months and afterward, the mechanical properties of each series were evaluated either. It is worth noting that to investigate the possibility of the occurrence of DSA during warm rolling experiments, $\ln(\dot{\varepsilon})$ vs. T^{-1} plot of the utilized steel was examined to assure whether the DSA

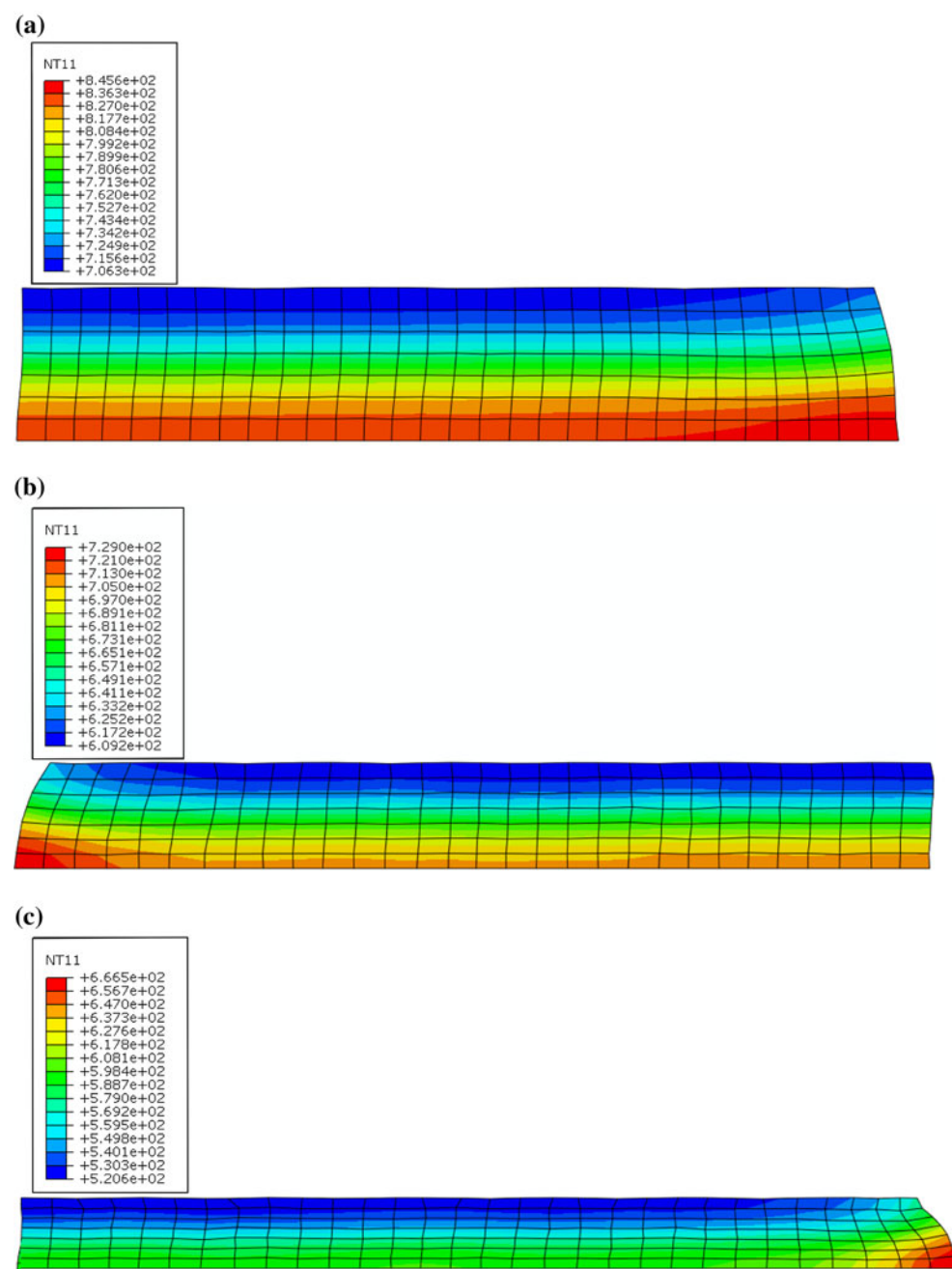
Fig. 2 **a** Effective strain distributions achieved by the employed model using the rolling layout in ref. [15], **b** average stress distribution achieved by the employed model using the rolling layout in ref. [15]



has taken place during the warm rolling experiments. In order to construct this graph, the tensile samples were prepared, and then tensile tests at various temperatures and strain rates were conducted. The experiments were performed at the temperatures in the range of 25–500 °C and the mean strain rates of 10^{-4} to 0.5 s^{-1} .

Finally, optical microscopy were also conducted to examine the microstructures for the samples rolled at various speeds and to study the microstructures within the warm-rolled samples.

Fig. 3 Temperature distribution during warm rolling at rolling speed of 43 rpm; **a** the first pass, **b** the second pass, and **c** the third pass



Results and discussion

In the first step, the results of the mathematical model have been verified using the published data. For instance, Fig. 2 displays effective strain rate and average stress distributions achieved by the proposed model using the rolling program in ref. [15] in which the initial temperature of 1,000 °C and reduction of 40% were employed. The model is performed for hot rolling of carbon steel using the flow stress data obtained in ref. [18]. It is seen that the

predictions are in good agreement with the results achieved by a finite-element model used in ref. [15].

After verification of the model results, the warm rolling process with the rolling conditions described in the previous section was modeled, for example, temperature distribution of the sample rolled at different rolling speeds, i.e., 43 and 71 rpm are presented in Figs. 3 and 4. Note that it was found that the employed steel shows serrated flow in the temperatures in the range of 100–450 °C. Figure 5a shows typical stress-strain curves obtained at 300 °C at

two different strain rates. Regarding the achieved stress-strain curves under different deformation conditions, the region of serrated flow was determined as a $\ln(\dot{\epsilon})$ vs. T^{-1} plot displayed in Fig. 5b. Considering the predicted temperature and strain rate distributions achieved from the model together with the $\ln(\dot{\epsilon})$ vs. T^{-1} plot shown in Fig. 5b, it is possible to determine the occurrence of DSA during warm rolling. According to Fig. 5b it can be observed that the employed rolling conditions are far from those required for the DSA to occur. It may be attributed to the relatively

Fig. 4 Temperature distribution during warm rolling at rolling speed of 71 rpm; **a** the first pass, **b** the second pass, and **c** the third pass

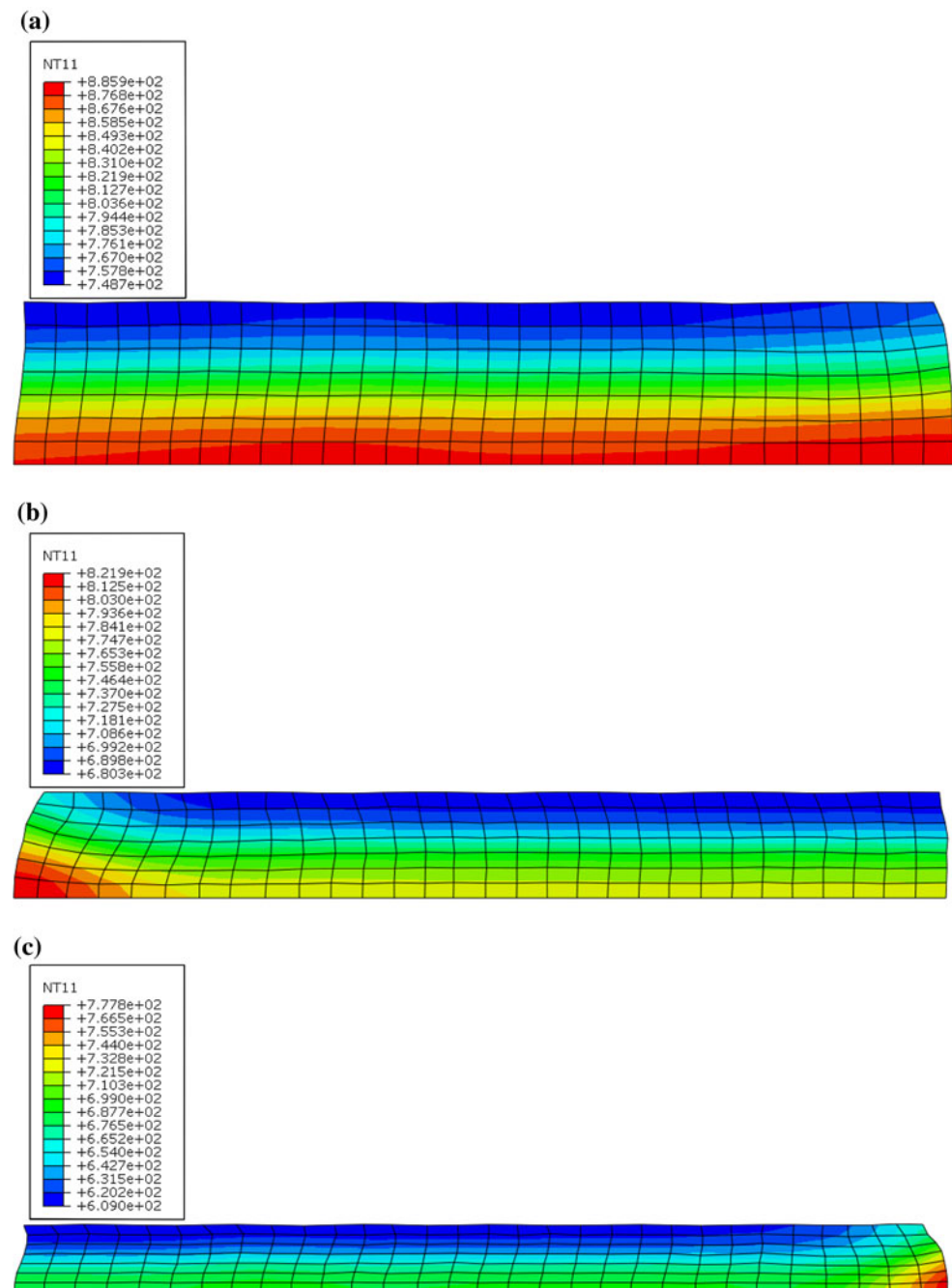


Fig. 5 **a** Typical stress–strain curves achieved from tensile testing at 300 °C, **b** regions of serrated and smooth flow according to the deformation temperature and applied strain rate

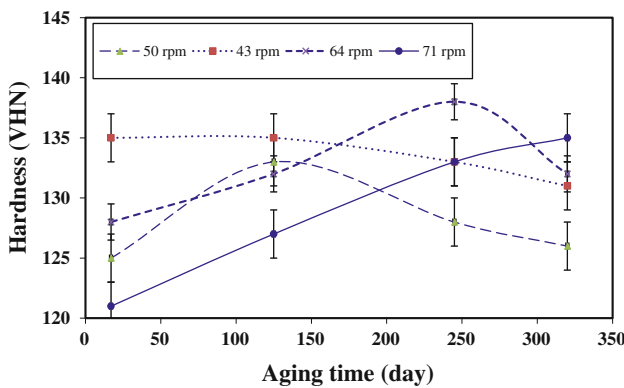
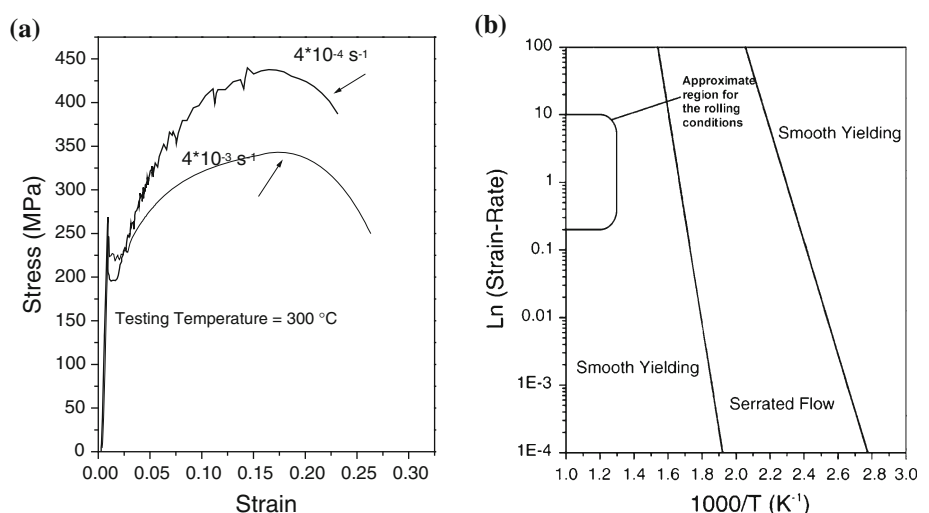


Fig. 6 Hardness versus aging time for warm-rolled samples with different rolling speeds

high initial temperature of the rolling material, which causes DSA, starts at very high strain rates. Thus, it can be stated that SSA only takes place after warm rolling.

In order to evaluate the kinetics of SSA, hardness and tensile tests were performed. Figure 6 represents the plots obtained from the results of Vickers hardness of warm-rolled samples at different aging times. It is obvious that static strain aging occurs in all samples, and as a result, the hardness increases, and even in the sample rolled at relatively lower rolling speed, i.e., 43 rpm, the hardness slightly decreases after 320 days. It is interesting to note that the time required for the samples to reach the hardness peak is varied with different rolling speeds, while the time required for the maximum hardness increases with increasing the rolling speed as displayed in Fig. 7. Note that the rolling speed can alter the temperature distribution of the warm rolled sample as displayed in Figs. 2 and 3, higher rolling speed causes higher temperatures in different regions of rolled metal. For instance, the maximum exit temperature under rolling speeds 43 and 71 rpm are about 665 and 775 °C, respectively. This also affects the concentration of

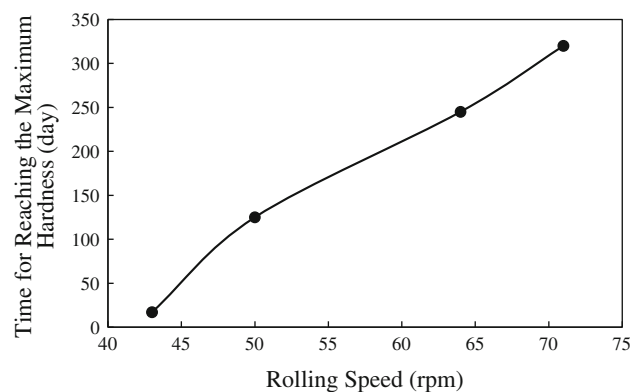


Fig. 7 Time required for reaching the maximum hardness at different rolling speeds

interstitial atoms in solution, i.e., carbon and nitrogen which are responsible for occurring static strain aging.

It is possible that partial static recrystallization occurs after warm rolling at higher rolling speeds. Therefore, it is expected that the hardness decreases as the rolling speed increases. This is particularly true for the as-received warm-rolled conditions as observed in Fig. 6. However, depending on temperature distribution at the end of warm rolling, the amount of static recrystallization during cooling to room temperature, and aging time it is possible that the hardness increases due to SSA. For instance, the maximum hardness value for the sample rolled at 43 rpm is greater than that of the sample rolled at 50 rpm just after warm rolling and even after aging for 320 days. On the other hand, the sample rolled at 64 rpm initially shows lower hardness, but after aging for 250 days, its hardness is higher than that for the sample rolled at 43 rpm. Therefore, it is concluded that there is an optimum rolling speed for acquiring the maximum hardness after warm rolling. Figure 8 shows the stress–strain curves of the samples rolled at 43 and 71 rpm. Figure 9 represents the variations of UTS of the aged

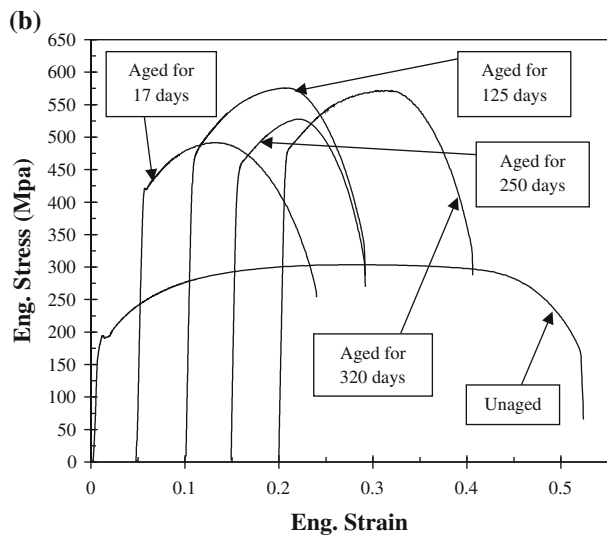
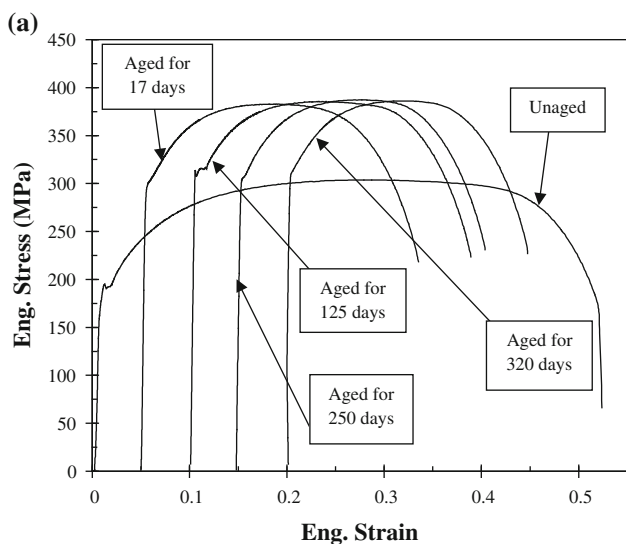


Fig. 8 Stress–strain curves obtained from tensile tests for the sample rolled at **a** 43 rpm, **b** 71 rpm

samples as a function of aging time. Figures 8 and 9 approve that SSA has taken place during the period of aging time and it has had significant effects in the mechanical behavior of the warm-rolled samples. In addition, it is also observed that the required time for the maximum yield stress and UTS increases by increasing the rolling speed.

Microstructural studies using optical microscopy has been conducted on the warm-rolled samples. Figure 10 shows the final microstructures of the samples rolled at 43 and 71 rpm. As mentioned above, the figure shows that partial static recrystallization occurs within the sample rolled at higher rolling speeds, i.e., 71 rpm. It should be noted that static recrystallization occurs particularly at the depth of the strip where the temperature is high enough to prompt recrystallization. Therefore, slower rate of strain

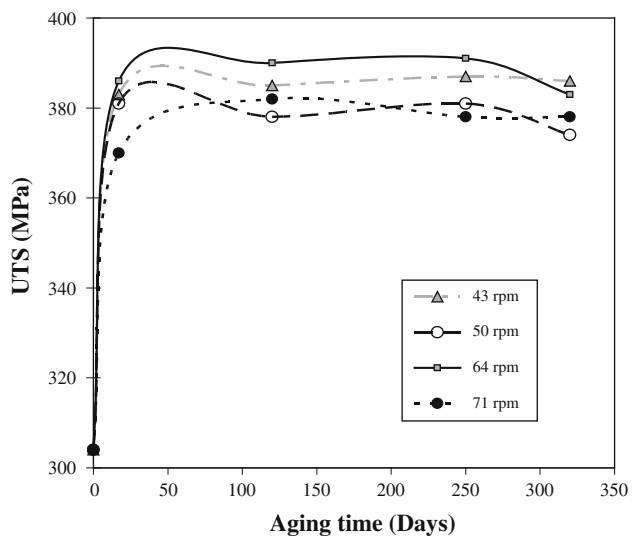


Fig. 9 UTS variations as a function of aging time for the warm-rolled samples

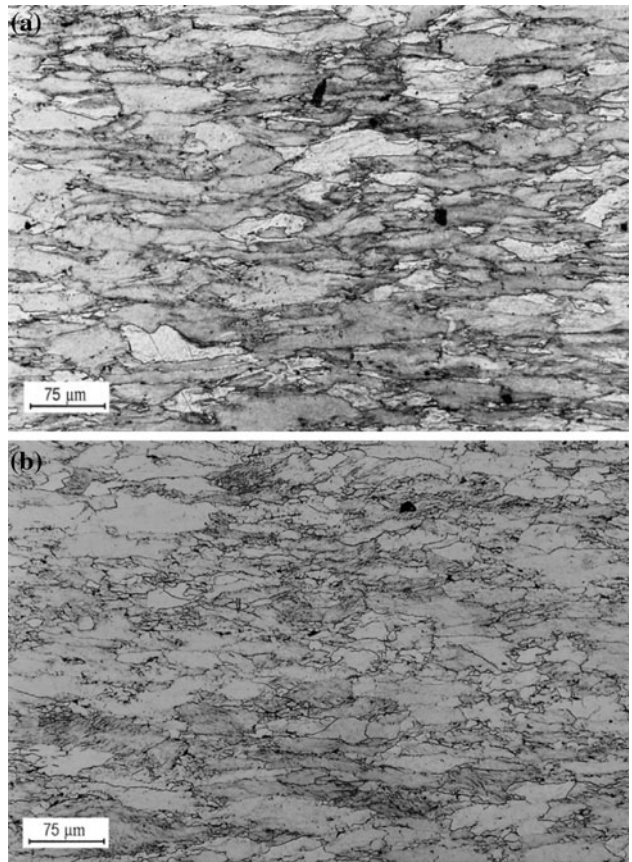


Fig. 10 Optical microstructures of the sample rolled at **a** 43 rpm, **b** 71 rpm

aging at rolling speed of 71 rpm may be attributed to occurrence of partial static recrystallization. In other words, it causes the decreasing of mobile dislocation density that is vital for taking place of SSA.

Conclusions

In this study, effect of rolling speed on strain aging within a low-carbon steel in warm rolling process has been studied. A two-dimensional finite-element model and the warm rolling experiments have been utilized to evaluate DSA and SSA phenomena. The results indicate that DSA may not occur for the employed rolling program; however, SSA occurs after warm rolling leading to changes in the mechanical behavior of the warm-deformed samples. The results show that rolling speed may significantly change the microstructures of the warm-rolled steel as well as alter the kinetics of subsequent SSA. By increasing the rolling speed from 43 to 71 rpm, the time needed for the occurrence of SSA increases from 17 days to more than 10 months. Thus, the desired mechanical properties in the warm-rolled steel may be achieved using a proper rolling layout and subsequent SSA phenomenon.

References

1. Robinson JM, Shaw MP (1994) Int Mater Rev 39:113
2. Leslie WC (1983) The physical metallurgy of steels. McGraw Hill, Tokyo
3. Mura T, Lautenschlager EA, Brittain JO (1961) Acta Metall 9:453
4. Hall EO (1970) Yield point phenomenon in metals and alloys. Macmillan, London
5. Staiger MP, Brownrigg A, Hodgeson PD, Davies CHJ (2004) Mater Sci Eng A 364:35
6. Pan CL, Wu S, Yu WW (2001) Thin-Walled Struct 39:429
7. Taheri AK, Maccagno TM, Jonas JJ (1995) Mater Sci Eng 11:1139
8. Taheri AK, Maccagno TM, Jonas JJ (1995) Metall Mater Trans A 26:1183
9. Gorni AA, Mei PR (2008) J Mater Process Technol 197:374
10. Gunduz S (2008) Mater Sci Eng A 486:63
11. Li CC, Leslie WC (1978) Metall Trans A 9:1765
12. Humphreys AO, Liu DS, Toroghinezhad MR, Jonas JJ (2002) ISIJ Int 42(Supplement):S52
13. Gonzalez BM, Marchi LA, Fonseca EJ, Modenesi PJ, Buono VTL (2003) ISIJ Int 43:428
14. Serajzadeh S (2004) Mater Sci Eng A 371:318
15. Lenard JG, Pietrzyk M, Cser L (1999) Mathematical and physical simulation of the properties of hot rolled products. Elsevier, Oxford
16. Dunne F, Petrinic N (2006) Introduction to computational plasticity. Oxford University Press, New York
17. Hibbitt (2004) ABAQUS User's Manual, Version 6.5, ABAQUS Inc., USA
18. Prasad YVRK, Sasidhara S (eds) (1997) Hot working Guide, ASM International, Materials Park, OH 447073-0002